

High-resolution Electron Microscopy of a Sr-containing Sialon Polytypoid Phase

J. Grins,^{a*} S. Esmailzadeh,^a G. Svensson^b and Z. J. Shen^a

^aDepartment of Inorganic Chemistry, Arrhenius Laboratory, Stockholm University, SE-106 91 Stockholm, Sweden

^bDepartment of Structural Chemistry, Arrhenius Laboratory, Stockholm University, SE-106 91 Stockholm, Sweden

(Received 28 January 1999; accepted 26 March 1999)

Abstract

A new type of Sr-containing sialon polytypoid phase with the structural formula $\text{SrSi}_{10-x}\text{Al}_{18+x}\text{N}_{32-x}\text{O}_x$ ($x \approx 1$) has been found in the Sr–Si–Al–O–N system. The phase was characterised by X-ray powder diffraction (XRPD), and its structure was investigated by electron diffraction (ED) and high resolution electron microscopy (HREM). It is considerably disordered, but the average structure has a rhombohedral unit cell with $a = 5.335(5) \approx \sqrt{3} \cdot a_{\text{AlN}}$ and $c = 79.1(1) \text{ \AA} \approx 30 \cdot c_{\text{AlN}}$. The Sr atoms are located in layers M–Sr–M, $M = (\text{Si}/\text{Al})$, at the origin of the unit cell with 12 X = (O,N) atoms around it, at distances of $\sim 3 \text{ \AA}$, forming a cubo-octahedron. The X atoms that form a hexagon around the Sr atom in the ab plane are corner shared by $M = (\text{Si}/\text{Al})$ tetrahedra with opposite polarity in adjacent layers in which 2/3 of the tetrahedra are occupied. The M–Sr–M layers alternate with normally eight-layer-thick AlN type blocks, although the thickness of these blocks frequently varies. The structural model obtained from the HREM images includes a polarity reversal of the tetrahedra in the AlN blocks, similar to that proposed to occur in Si–Al–O–N polytypoid phases. The model with one Sr layer and 10 $M = (\text{Si}, \text{Al})$ layers per 1/3 of the repeat unit agrees with the composition of the phase and experimental HREM images. © 1999 Elsevier Science Ltd. All rights reserved

Keywords: strontium, sialon, polytypoid, electron microscopy.

1 Introduction

The Si–Al–O–N (sialon) polytypoid phases occur near the AlN-rich corner of the Si_3N_4 – SiO_2 – Al_2O_3 –AlN system diagram.^{1,2} They have similar

layer structures that vary systematically with their composition, and which have therefore been assigned the name polytypoids in order to distinguish them from polytype phases which preserve a constant, or nearly constant, chemical composition. The structural characterisation of the phases has been reviewed by Thompson *et al.*^{3,4} They are rhombohedral or hexagonal with *a* axes in the range 2.99–3.08 Å and are designated by Ramsdell symbols, e.g. 8H or 27R. The rhombohedral nR Si–Al–O–N polytypoids consist of three structurally related blocks of n/3 layers and the hexagonal nH polytypoids of two n/2 blocks. The fundamental block in each member of the series, and thus that of the phase, has the composition M_mX_{m+1} , or $\text{MX}_{(m+1)/m}$, with $M = (\text{Si}, \text{Al})$ and $X = (\text{O}, \text{N})$, and observed values for *m* include 4, 5, 6, 7, 9 and 11. The Si/Al ratio in the phases is variable due to the substitution mechanism $\text{Si}^{4+} + \text{N}^{3-} \leftrightarrow \text{Al}^{3+} + \text{O}^{2-}$, e.g. for the 27R phase theoretically from a pure Al composition, $\text{AlNO}_{1/9}$, to $\text{Si}_{3/9}\text{Al}_{6/9}\text{N}_{10/9}$ (67% Al). According to the currently accepted model, the structures contain close packed hexagonal AlN or wurtzite type MX layers that are modified by two additional features, as shown in Fig. 1: (i) in each block of the structure there is one MX layer with Al atoms at octahedral sites; (ii) in between the octahedral layers there are layers in which the M atoms statistically occupy 50% of sites shared by two adjacent face-sharing tetrahedra. The second feature effects a polarity reversal of the AlN layers so that those connected to the octahedral MX layers on both sides of it point in opposite directions. Structural studies of these phases have mainly been carried out using HREM,^{5–10} and proposed structural models have been confirmed by XRPD in a few cases.^{4,8} The models differ in details of the arrangement in the AlN type layers, which have so far not been established with certainty, however. The regions or blocks in polytypoid structures that contain the close packed hexagonal MX layers will hereafter be

*To whom correspondence should be addressed. E-mail: mat@inorg.su.se

designated as AlN type, although these regions may be modified by additional features. Bando *et al.*⁸ have shown by using convergent beam electron diffraction that the space groups for the 12H and 15R polytypoids are both non-centrosymmetric, $P6_3mc$ and $R3m$, respectively, contrary to earlier belief.

Other cations with smaller ionic radii, like Li^+ , Be^{2+} , Mg^{2+} , and Sc^{3+} , can be incorporated into tetrahedral or octahedral sites in the structures of the sialon polytypoid phases,³ possibly causing additional structural modifications. It has been commonly believed that larger cations that do not fit into, e.g. the octahedral sites, cannot be incorporated, but experimental evidence has nevertheless indicated the formation of a hexagonal polytype-resembling faulted phase in the Sr-doped sialon system,¹¹ with an Sr content of 2 at% and a ~ 25 Å spacing along 000 l , but its structure was not clarified in the study.

In a systematic work related to the preparation and study of the stability of a series of α -sialons, $\text{Me}_x\text{Si}_{12-(m+n)}\text{Al}_{(m+n)}\text{O}_n\text{N}_{16-n}$ with $\text{Me} = \text{Ca}, \text{Sr}, \text{Y}$, and rare-earth elements, we confirmed the formation of an Sr-containing polytypoid phase in the Sr-doped sialon system¹² and found evidence for the existence of similar phases with other large cations, e.g. Eu^{13} and La (unpublished). It seems clear that these cations are too large to be accommodated

into tetrahedral or octahedral sites and that they have a different atomic surrounding than those found for cations in the polytypoid phases structurally characterised so far. The present study comprises an HREM investigation of one such Sr-containing phase and a derivation of a structural model for it that agrees with its composition and experimental HREM images.

2 Experimental

The cation ratio in the Sr-containing polytypoid phase was initially determined by energy dispersive spectrometer (EDS) analysis in a scanning electron microscope (SEM), for crystals in a sample with the nominal composition $\text{Sr}_{0.6}\text{Al}_{2.5}\text{Si}_{9.6}\text{O}_{1.2}\text{N}_{14.8}$, prepared by hot-pressing at 1800°C for 2 h. Besides the polytypoid phase it contained α - and β -sialon and the S-phase $\text{Sr}_2\text{Al}_x\text{Si}_{12-x}\text{N}_{16-x}\text{O}_{2+x}$ ($x \approx 2$).¹² A series of specimens mimicking the EDS-determined composition were subsequently prepared in order to obtain this new phase as pure as possible. The sample used for structural characterisation had a nominal composition of $\text{SrSi}_5\text{Al}_{11}\text{O}_2\text{N}_{17}$ and contained more than 95 vol% of the desired phase. It was prepared from an appropriate mixture of powders of Si_3N_4 (UBE, SN-E10), AlN (H.C. Starck-Berlin, grade A), and SrCO_3 (99.0%, Allied Chemical, NY). Corrections were made for the oxygen present in the Si_3N_4 and AlN raw materials, corresponding to 2.7 and 1.9 wt% SiO_2 and Al_2O_3 , respectively. The precursor powders were ball-mixed in propanol for 24 h. The dried powder mixture was then hot-pressed in nitrogen atmosphere at 1800°C and 35 MPa for 2 h in a graphite resistance furnace. The prepared sample was characterised by its XRPD pattern, obtained with a Guinier-Hägg camera, using $\text{CuK}\alpha_1$ radiation and Si as internal standard. Its microstructure was

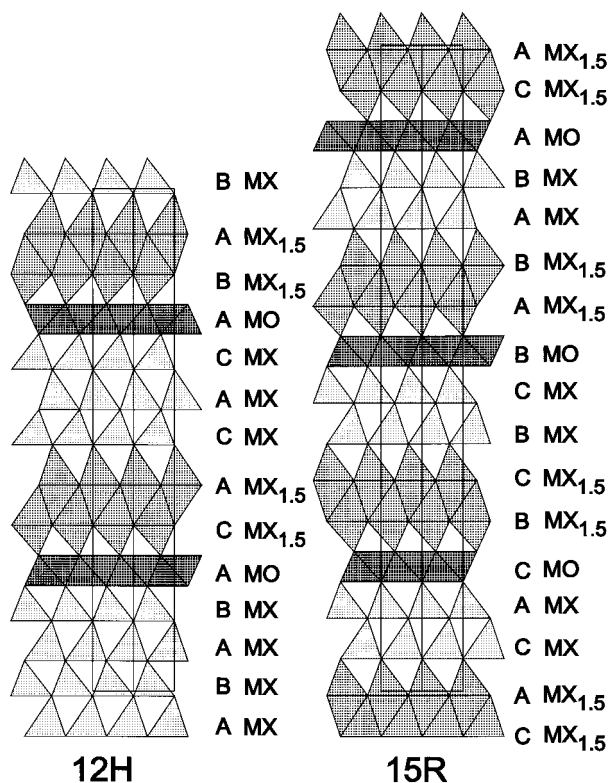


Fig. 1. Polyhedral illustrations of 12H and 15R Si-Al-O-N polytypoid phases viewed along [110]. The packing sequence of the metal atoms and the composition of each metal layer per unit cell are indicated. Adapted from Ref. 8.

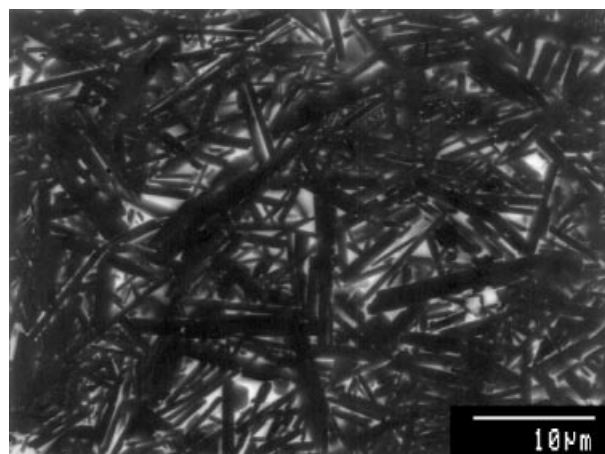


Fig. 2. SEM back-scatter electron image of an Sr sialon sample with nominal composition $\text{SrSi}_5\text{Al}_{11}\text{O}_2\text{N}_{17}$.

examined in a JEOL JSM 880 SEM, equipped with an EDS microanalysis system LINK AN10000. The quantitative EDS analyses were made using the ZAF-4 software and measured metal standard spectra. Additional EDS analyses were performed in a transmission electron microscope (TEM) JEOL 2000FX with an EDS system LINK QX200 and the detector situated at a high-angle position.

HREM images were recorded with a TEM JEOL 3010, operated at 300 kV and with an optimal resolution of 1.7 Å. Theoretical images for different crystallite thickness and defocus values were calculated with the program MacTempas.¹⁴

3 Results

Figure 2 shows an SEM back-scatter electron image from a polished and carbon-coated surface of the sample with nominal composition $\text{SrSi}_5\text{Al}_{11}\text{O}_2\text{N}_{17}$. The crystallites of the polytypoid phase are needle shaped, with lengths and diameters of ca 10–50 and 1–5 μm , respectively, and are surrounded by a more Sr-rich amorphous phase. An average of 20 EDS point analyses yielded a metal composition of 3.4(3)% Sr, 31(1)% Si and 66(2)% Al. The composition was later confirmed by EDS analysis of individual grains in the TEM. The Si/Al content is thus found to be similar to that of, e.g. an Si-rich 27R polytypoid phase.

Electron diffraction patterns of the Sr polytypoid phase are shown in Fig. 3. They correspond to a rhombohedral unit cell with $a \approx 5.3 \text{ \AA} \approx \sqrt{3} \cdot a_{\text{AlN}}$ and $c \approx 79 \text{ \AA}$. The a axis is thus found to be ca. $\sqrt{3}$ times that of the Si–Al–O–N polytypoid phases. The streaking seen along c^* in the $\langle 100 \rangle$ and $\langle \bar{1}10 \rangle$ patterns implies structural disorder. The disorder breaks the symmetry and gives rise to the weak reflections in the $\langle 001 \rangle$ pattern that are forbidden for a rhombohedral lattice.

HREM images of the Sr-phase taken along $\langle 100 \rangle$ and $\langle \bar{1}10 \rangle$ are shown in Fig. 4. There are two distinct features in the well-ordered fragment viewed along $\langle 100 \rangle$: regions containing eight dark layers and darker regions with a thickness of approximately three of the former layers. A closer inspection of the latter shows them to consist of three rows of dark spots. The image contrast in the eight-layer regions is similar to that observed in experimental or calculated HREM images of Si–Al–O–N polytypoid phases. The distance between the layers, $\sim 2.6 \text{ \AA}$, is furthermore in agreement with that observed for the latter phases. These regions, or blocks, can therefore be concluded to consist essentially of close-packed AlN (wurtzite) type layers. The projected periodicity of the

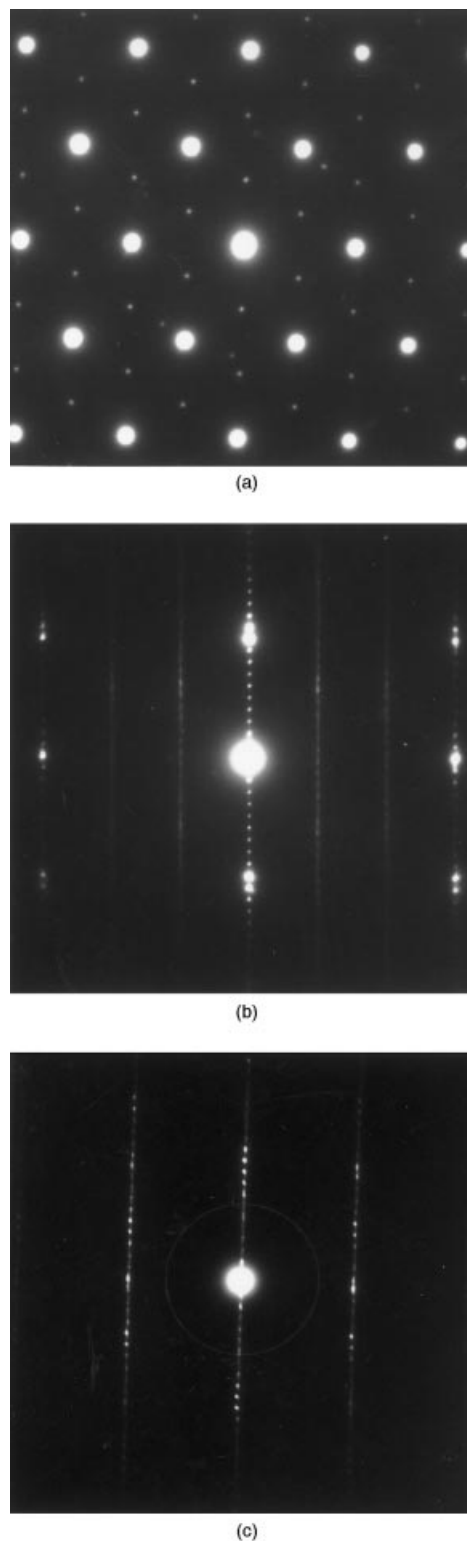


Fig. 3. ED patterns of the Sr polytypoid phase along (a) $\langle 001 \rangle$, (b) $\langle 110 \rangle$ and (c) $\langle 100 \rangle$. They correspond to an average rhombohedral unit cell with $a = 5.3$ and $c = 79 \text{ \AA}$. The streaking along c^* implies disorder in that direction. The weak reflections in (a) are forbidden for a rhombohedral lattice and are caused by the disorder along c^* that breaks the symmetry. The reflection condition $h-hl:l=3n$ is clearly seen in the $\langle 100 \rangle$ pattern in (a), and the reflection condition $00l:l=3n$ in the ED patterns in (b) and (c).

$M = (\text{Si}, \text{Al})$ or $X = (\text{O}, \text{N})$ sites perpendicular to the c -axis is accordingly $\sim 1.5 \text{ \AA}$, i.e. below the resolution of the microscope, and that in the darker three-layer band is $a \cdot \cos(30^\circ) \approx 4.6 \text{ \AA}$.

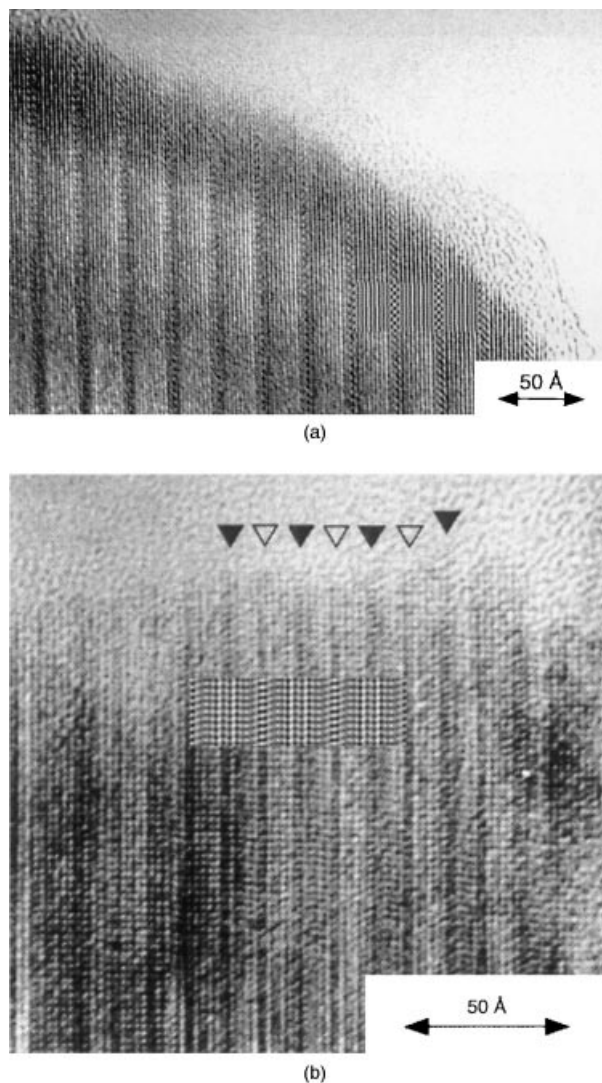


Fig. 4. HREM images of the Sr polytypoid phase along (a) $\langle 100 \rangle$ and (b) $\langle 110 \rangle$ with calculated images inserted. The triangular markings in (b) are explained in the text.

The HREM image in Fig. 4(b), taken along $\langle 110 \rangle$ shows regions with a nearly square net of dots at intervals of ~ 2.4 Å along the c axis and 2.7 Å perpendicular to it, similar to that observed for the Si–Al–O–N polytypoids described above. These regions are separated by two alternating darker bands, marked by open and filled triangles in the figure. Those marked with open triangles exhibit a contrast similar to that observed for the double $\text{MX}_{1.5}$ layers in the Si–Al–O–N polytypoids^{5–10} (see Fig. 1). These bands together with the adjacent layers on both sides of them are thus concluded to be of AlN type. Associated with the layers marked with filled triangles, a tilt in the contrast can be seen. This indicates that the hexagonal close packing in the AlN type part, corresponding to straight rows of dark dots, is in this part replaced with a cubic close packing of metal or anion layers. These cubic close packed layers most likely correspond to the darker three-layer-broad band in the images along $\langle 100 \rangle$, and it is reasonable to assume that the Sr atoms are located

here. This inference is further supported by the somewhat darker contrast observed for them.

A partial structural model for the Sr-containing polytypoid phase can be derived from considerations of its composition and site preferences for the metal atoms, in particular Sr. The Sr content of ca 3.4%, as obtained from EDS analysis, indicates that each three-layer-thick band contains only one Sr atom per unit cell. It must thus be located at the special position (0,0,0) and partly define the periodicity in the ab plane. The oxygen arrangement around the Sr atoms is furthermore expected to have Sr–X distances of ca. 3 Å and to fit well with adjacent AlN type layers. Since the ionic radius of Sr^{2+} is similar to that of $\text{O}^{2-}/\text{N}^{3-}$, the perhaps most obvious possibility to consider is that of SrX_2 layers with each Sr atom surrounded by a hexagon of X atoms, as is found in many structures, including those derivable from the cubic perovskite type. If that is the case, and if the anions in this layer are in addition shared between two tetrahedrally coordinated M atoms, i.e. if they are not apical, then the tetrahedra of the latter must point in opposite directions along the c axis. A model for the three-layer band accordingly consists of $\text{M}_2\text{X}_{2.5}\text{-SrX-M}_2\text{X}_{2.5}$ layers, as shown in Fig. 5. The triangles of X atoms that constitute the bases of the tetrahedra in the two layers can be identically oriented or rotated 60° relative to each other around the c axis. The latter arrangement is here considered more likely, since the coordination polyhedron for the Sr atom then is a cubo-octahedron, a common configuration of oxygen atoms around Sr, with 12 X atoms at approximately equal distances of ca 3 Å. Since the polarities of the tetrahedral layers on both sides of the SrX layer are opposite, a polarity reversal of tetrahedra must take place in the regions containing the eight AlN type layers. The experimental images taken along $\langle 100 \rangle$ give relatively little information about the details in these parts of the structure, while those taken along $\langle 110 \rangle$ are more informative. As mentioned above, the rows of dots parallel with c^* appear to be straight in the image along the latter direction, which suggests a hexagonal packing sequence B–A–B–A for the metals. The shift at the layers marked with filled triangles indicates furthermore a cubic close packing of anions around the Sr atoms, in agreement with the structural model. The polarity reversal of tetrahedra that must take place in the AlN type block can be accomplished by the presence of two adjacent metal layers with composition $\text{M}_3\text{X}_{4.5}$, of the type found to occur, e.g. in the 15R sialon polytypoid phase.^{3,8} The dark layers marked with open triangles would consequently correspond to the position of these layers. The metal atoms in them accord-

ingly occupy randomly 50% of the sites in tetrahedra that share faces, in such a way that in no pair of two face-sharing tetrahedra both contain a metal atom. For visualisation, the layers may also be seen as metals fully occupying sites coordinated by trigonal bipyramids of X atoms, although the equatorial M–X distances then become unrealistically short. An insertion of two $M_3X_{4.5}$ layers in the eight-layer regions can occur in different positions, giving different numbers on both sides of adjacent MX layers. The dark layers marked with open triangles in the HREM images indicate however that the two $M_3X_{4.5}$ layers are symmetrically placed in the middle of the eight-layer region. Using the three unit layer types; $M_2X_{2.5}$ –SrX– $M_2X_{2.5}$, M_3X_3 (MX) and $M_3X_{4.5}$, a model structure can be built as shown in Fig. 6. The corresponding packing sequence for the metals is C–C(Sr)–C–A–B–A–B–A–B–A–B–C–C(Sr)–C, and the average height for a tetrahedral layer is $79.1/30 = 2.64$ Å. The symmetry for the idealised model is $R\bar{3}$, $a = 5.335(5)$, and atomic coordinates for it are given in Table 1. The unit cell parameters were obtained from Guinier–Hägg film data (see below).

To verify the structural model a series of HREM images along $\langle 100 \rangle$ and $\langle \bar{1}10 \rangle$ were calculated, using the atomic coordinates in Table 1. The following instrument parameters were used; 300 kV, objective aperture = 0.5 \AA^{-1} , convergence angle = 0.550° , mechanical vibration = 0.3, $C_s =$

0.7 and Gaussian spread of focus = 50 \AA . The best correspondence between observed and calculated images was found close to the Scherzer focus at -350 \AA for all calculated thicknesses. Calculated images for a thickness of 20 \AA is shown in inserts in Fig. 4. The agreement is satisfactory, considering that only an idealised model is used, in particular with respect to the 3-layer band containing Sr.

A composition for the proposed structural model can be calculated as follows: in one third of the unit cell there are two layers of tetrahedrally coordinated metal atoms surrounding the Sr atoms, with a total content of M_4X_5 , six wurtzite type layers with summed composition $M_{18}X_{18}$ and two layers with partial metal occupancies of tetrahedral sites and a summed content M_6X_9 , yielding the structural formula $SrM_{28}X_{32}$ or $Sr_{0.036}MX_{1.145}$. If all X atoms are assumed to be nitrogen, the composition $SrSi_{10}Al_{18}N_{32}$ is obtained, by charge balancing, with a metal content of 3.4% Sr, 34.5% Si and 62.1% Al. Considering formal valencies it is furthermore tempting to assume only Al in the AlN-type layers and only Si in the other two types of layers. The quantitative EDS analysis yielded a metal content of 3.4(3)% Sr, 31(1)% Si and 66(2)% Al, which corresponds to the formula $Sr_{1.0(1)}Si_{8.9(3)}Al_{19.1(6)}N_{30.9}O_{1.1}$ (with the N and O content derived by charge balancing), i.e. one with a slightly lower Si/Al ratio. It is likely that the Si/Al ratio can vary as in other polytypoid phases,

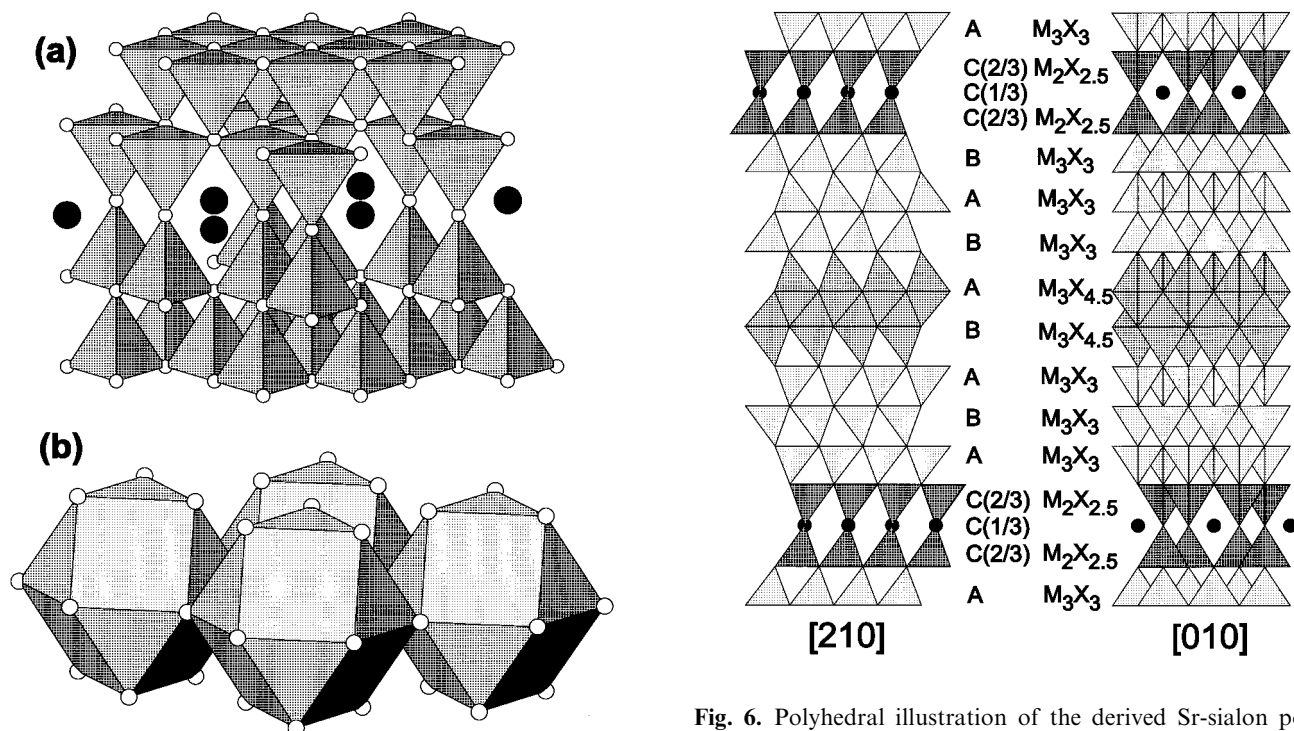


Fig. 5. (a) An illustration of the structural model for the three-layer ($Si_2X_{2.5}$ –SrX– $Si_2X_{2.5}$) region containing Sr. The Sr atom positions are shown by filled circles. (b) An illustration of the cubo-octahedra of anions around the Sr atoms.

Fig. 6. Polyhedral illustration of the derived Sr-sialon polytypoid structure viewed along $[210]$ and $[010]$, with corresponding atomic coordinates given in Table 1. The Sr atoms are shown by filled circles. The packing sequence of the metal atoms and the composition of each metal layer per unit cell are indicated.

however, due to the substitution $\text{Si}^{4+} + \text{N}^{3-} \leftrightarrow \text{Al}^{3+} + \text{O}^{2-}$, implying the more general structural formula $\text{SrSi}_{10-x}\text{Al}_{18+x}\text{N}_{32-x}\text{O}_x$. The composition derived from the EDS analysis, $\text{Sr}_{1.0(1)}\text{Si}_{8.9(3)}\text{Al}_{19.1(6)}\text{N}_{30.9}\text{O}_{1.1}$, thus agrees within error with a composition $\text{SrSi}_{8.9}\text{Al}_{19.1}\text{N}_{30.9}\text{O}_{1.1}$ ($x=1.1$) that conforms with the structural model. The observed variation of the number of layers in the regions not containing Sr, see below, may also produce a somewhat different composition than that of the average structure.

The streaking along c^* in the ED patterns indicates a high degree of disorder in the crystallites. Just a glance at the structural model suffices to make one expect variations in the width of the AlN type blocks, which also was the observed case for most crystallites (see Fig. 7). In this HREM image the number of metal layers in the AlN type block varies between 6 and 11. When the number is even

Table 1. Atomic coordinates for the idealised structure model for the Sr polytypoid phase ($M=(\text{Si},\text{Al})$, $X=(\text{O},\text{N})$, space group $R\bar{3}$, $a = 5.335(5)\text{\AA}$ and $c = 79.1(1)\text{\AA}$)

Atom	x	y	z	s.o.f
Sr	0	0	0	1.0
M1	2/3	1/3	0.02300	1.0
M2	2/3	1/3	-0.02300	1.0
M3	1/3	0	0.05303	1.0
M4	1/3	1/3	0.08333	1.0
M5	1/3	0	0.11364	1.0
M6	1/3	1/3	0.14519	0.5
M7	1/3	1/3	0.15731	0.5
X1	0	1/3	0.03030	1.0
X2	1/3	1/3	0.06060	1.0
X3	0	1/3	0.09090	1.0
X4	1/3	1/3	0.12120	1.0
X5	0	1/3	0.15150	1.0
X6	0	0	0.33333	1.0

there is a relative shift of two neighbouring Sr-containing layers by 1/3 of the periodicity perpendicular to the c axis, in agreement with the rhombohedral model shown in Fig. 6. When the number is odd no such shift is observed, as marked in the image. A corresponding seven-layer model structure, built from the structural units described above and with symmetry $P6_3cm$, is shown in Fig. 8(a). However, for one of the AlN type blocks with seven metal layers, marked in the image, two Sr layers are nevertheless shifted relative to each other. A corresponding model structure with the Sr layers shifted by 1/3 along $\langle 1\ 2\ 0 \rangle$ is shown in Fig. 8(b). In this case the anions around the Sr atoms are hexagonally instead of cubically close packed. A different kind of observed defect is shown in Fig. 9, where the Sr layer is interrupted and shifted along the c axis, resulting in a change of the width of the AlN type blocks between the Sr-layers.

Guinier-Hägg XRPD patterns of different preparations of the Sr polytypoid phase contained strong reflections that could be indexed with an AlN type hexagonal unit cell, with $a = 3.081(2)$ and $c = 5.242(8)\text{\AA}$, and in addition a number of reflections with relative intensities below 20%, most of them with intensities about 2–6%. The number of additional reflections varied for different preparations between ca 25 and 70, and so did also many of their positions and intensities. Most of the reflections at lower 2θ values could be accounted for by a rhombohedral unit cell corresponding to the structure model derived from HREM images with $5.335(5)$ and $79.1(1)\text{\AA}$, and some additional ones by a primitive hexagonal unit cell with the same dimensions. The agreement between inten-

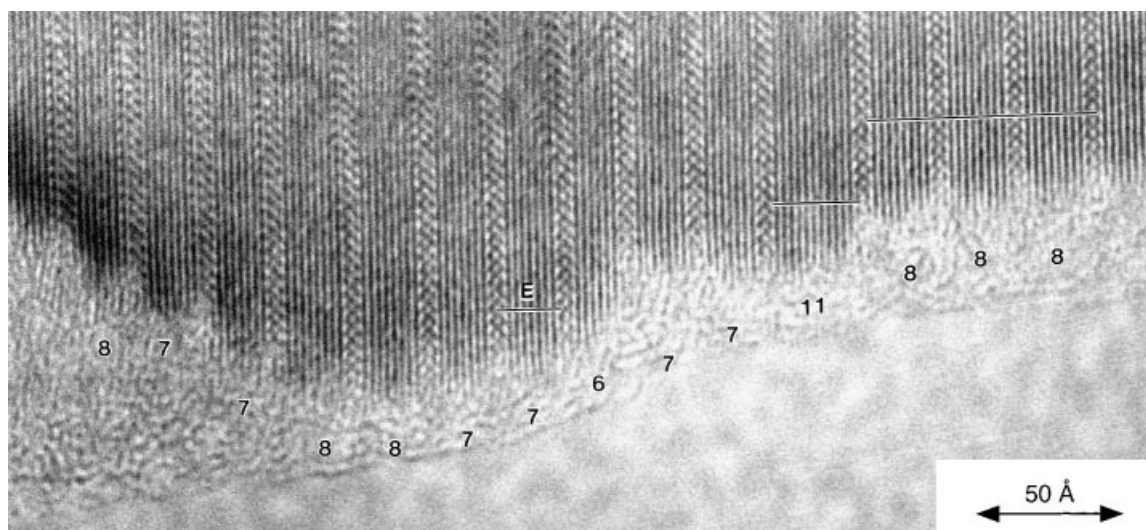


Fig. 7. HREM image along $\langle 100 \rangle$ of a disordered crystallite of the Sr sialon polytypoid phase. The widths of the AlN type regions are designated and the shift of the Sr containing layers emphasised by lines. Parts with an even number of metal layers comply for the most part with rhombohedral symmetry and a shift of subsequent Sr layers. This is normally not observed for an odd number of metal layers between the Sr layers. An exception from this is marked with an E.

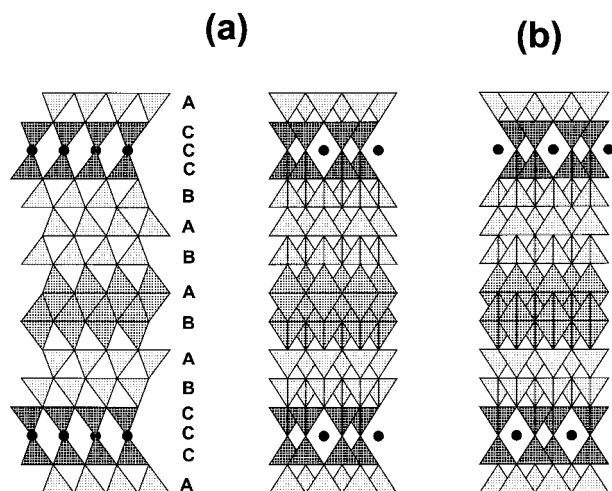


Fig. 8. (a) Structural model of an Sr polytypoid phase with seven metal layers in the AlN type block and symmetry $P6_3cm$, illustrated along $\langle 100 \rangle$ and $\langle \bar{1}10 \rangle$. (b) A corresponding model with one Sr layer shifted by $1/3 \langle 120 \rangle$.

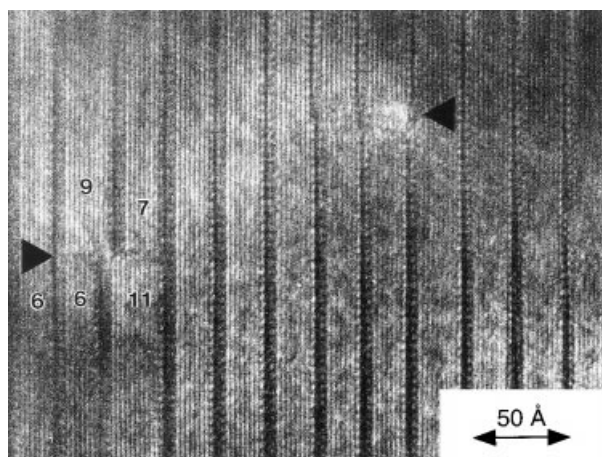


Fig. 9. An HREM image of the Sr polytypoid phase along $\langle 100 \rangle$, showing a defect consisting of a break and shift of an Sr-containing layer.

sities in the observed XRPD patterns and a calculated pattern for the structural model was found to be poor, however, in particular at lower 2θ values where the calculated pattern contained reflections with appreciable intensities which were all absent, or of much lower intensities, in the observed patterns. In some of the patterns the first observed reflection is found at a d value of 2.69 \AA , and all reflections of the $00l$ type and most of the $10l$ type are thus absent or too weak to be observed. The extensive faulting observed in the HREM images is however expected to alter the reflection intensities considerably from that of an ordered phase, and the observed patterns are difficult to interpret without actually computing the effect of the faults.¹⁵ An example of a similar effect of faulting on reflection intensities is illustrated by the disordered $2H^8$ sialon polytypoid phase.³ It has the composition $M_{11}X_{12}$, and in the structure there are

layers with composition MX_2 incorporated randomly at an average separation of 11 layers of tetrahedra. As a consequence of the disorder, however, the XRPD pattern contains only AlN-type reflections.

4 Concluding Remarks

The compound $Sr_{1.0}Si_{8.9}Al_{19.1}N_{30.9}O_{1.1}$ reported here is the first structurally characterised Sr-containing sialon polytypoid phase. The HREM study shows that Sr can enter this type of structure by forming layers containing SrX_{12} cubo-octahedra and MX_4 tetrahedra. A structural model has been derived that contains these layers alternating with AlN type blocks into which $M_3X_{4.5}$ layers are incorporated. The average width of the AlN type blocks corresponds to eight metal layers, although variations of this number were frequently observed in the HREM images. It is possible that similar ordered phases may exist with different compositions and numbers of metal layers in the AlN type blocks. Such phases would be members of an homologous series $(SrM_4X_5) \cdot (M_6X_9) \cdot (M_3X_3)_{n-2}$, with n being the number of layers between the SrM_4X_5 regions; and the present compound is described by $n=8$.

To obtain more detailed knowledge of the structure, diffraction studies of well-ordered, single-phase samples are needed. Whether it is possible to synthesise such with $n=8$ and/or for other values for n remains to be established. Related phases seem to exist for other cations with sizes similar to that of Sr^{2+} , and investigations of these have been initiated.

The structure of the Sr polytypoid phase is intimately connected with the wurtzite structure of AlN and the need for a 180° shift of the tetrahedra to fit the apex-linked tetrahedra in the layers containing Sr. For the present compound it is probable that this is accomplished by insertion of a double M_6X_9 layer in which base-sharing tetrahedra are 50% occupied by M atoms. Other possibilities of achieving the 180° shift are possible, however. The M atoms may for instance be centered in a triangular base of anions and thus have a trigonal bipyramidal coordination. The HREM simulations show that this is not the case for the Sr polytypoid phase, but the arrangement is found in structures of compounds of the type $(InFeO_3)(ZnO)_m$.^{16,17} In these a polarity reversal of MO_4 tetrahedra takes place in ZnO (wurtzite) type blocks that are separated by layers containing In atoms. The reversal in orientation takes place via a gradual shift of the M atoms in the MO_4 tetrahedra, and layers with MO_5 trigonal prisms are found halfway between $InO_{1.5}$

layers. When the value of m gets large, typically around 22, these layers break up and zigzag chains of MO_5 trigonal prisms form in the ZnO blocks.

Acknowledgements

The authors thank Dr T. Hörlin and Professor M. Nygren for valuable discussions.

References

- Gauckler, L. J., Lukas, H. L. and Petzow, G., Contribution to the phase diagram $\text{Si}_3\text{N}_4\text{-AlN-Al}_2\text{O}_3\text{-SiO}_2$. *J. Am. Ceram. Soc.*, 1975, **58**, 346–347.
- Jack, K. H., Sialons and related nitrogen ceramics. *J. Mat. Sci.*, 1976, **11**, 1135–1158.
- Thompson, D. P., Korgul, P. and Hendry, A., The structural characterisation of sialon polytypoids. In *Progress in Nitrogen Ceramics*, ed. F. L. Riley. Nijhoff, The Hague, The Netherlands, 1983, pp. 61–74.
- Thompson, D. P., The crystal structures of 8H and 15R sialon polytypes. In *Nitrogen Ceramics*, ed. F. L. Riley. Noordhoff, Leyden, The Netherlands, 1977, pp. 129–135.
- Hendry, A. and Jack, K. H., The electron microscopy of sialon ceramics. In Proc. 5th Polish Electron Microscopy Conference, Warsaw, 1978, pp. 397–405.
- Bando, Y., Matsui, Y., Kitami, Y. and Inomata, Y., An application of the JEM-4000EX high resolution analytical electron microscope. *JEOL News*, 1984, **22**, 28–32.
- Krishnan, K. M., Rai, R. S., Thomas, G., Corbin, N. D. and McCauley, J. W., Characterization of long period polytypoid structures in the $\text{Al}_2\text{O}_3\text{-AlN}$ system. *Mater. Res. Soc. Symp.*, 1986, **60**, 211–218.
- Bando, Y., Mitomo, M., Kitami, Y. and Izumi, F., Structure and composition analysis of silicon aluminium oxynitride polytypes by combined use of structure imaging and microanalysis. *J. Microscopy*, 1986, **142**, 235–246.
- Tanaka, H., Bando, Y., Inomata, Y. and Mitomo, M., Atomically sharp crack in 15R-sialon. *J. Am. Ceram. Soc.*, 1988, **71**, C32.
- Wang, H., Sun, H., Zhuang, H., Feng, J. and Yen, T. S., Microstructural observation of β' -sialon-12H multiphase ceramics by HREM. *Mat. Lett.*, 1993, **17**, 131–136.
- Hwang, C. J., Susnitzky, D. W. and Beaman, D. R., Preparation of multication α -SIALON containing strontium. *J. Am. Ceram. Soc.*, 1995, **78**, 588–592.
- Shen, Z. J., Grins, J., Esmailzadeh, S. and Ehrenberg, H., Preparation and crystal structure of a new Sr containing sialon phase $\text{Sr}_2\text{Al}_x\text{Si}_{12-x}\text{N}_{16-x}\text{O}_{2+x}$ ($x \approx 2$). *J. Mat. Chem.*, 1999, **9**, 1019–1022.
- Shen, Z. J., Nygren, M., Wang, P. and Feng, J., Eu-doped α -sialon and related phases. *J. Mater. Sci. Lett.*, 1998, **17**, 1703–1706.
- O'Keefe, M. A. and Kilaas, R., *Users Guide to NCEMSS*. National Center for Electron Microscopy, Materials Science Division, Lawrence Berkely Laboratory, University of California, 1994.
- Drits, V. A. and Tchoubar, C., *X-ray Diffraction by Disordered Lamellar Structures*. Springer-Verlag, Berlin, 1990.
- Li, C., Bando, Y., Nakamura, M. and Kimizuka, N., A modulated structure of $\text{In}_2\text{O}_3(\text{ZnO})_m$ as revealed by high-resolution electron microscopy. *Jap. Soc. Elec. Micr.*, 1998, **46**(2), 119–127.
- Hörlin, T., Svensson, G. and Olsson, E., Extended defect structures in zinc oxide doped with iron and indium. *J. Mater. Chem.*, 1998, **8**, 2465–2473.